Geochemistry Geophysics Geosystems G3

Article
Volume 14, Number 9
13 September 2013
doi: 10.1002/ggge.20210
ISSN: 1525-2027

Published by AGU and the Geochemical Society

Preeruptive flow focussing in dikes feeding historical pillow ridges on the Juan de Fuca and Gorda Ridges

I. A. Yeo
GEOMAR Helmholtz Centre for Ocean Research Kiel, Wischhofstr. 1-3, 24148, Kiel, Germany (iyeo@geomar.de)

D. A. Clague, J. F. Martin, J. B. Paduan, and D. W. Caress
Monterey Bay Aquarium Research Institute, Moss Landing, California, USA

[1] Linear, hummocky pillow mound volcanism dominates at slow and intermediate spreading rate mid-ocean ridges. Volcanic hummocks are thought to be formed by low effusion rates or as a result of flow focussing during effusive fissure style eruptions in which the initial dike intercepts the seafloor and erupts along its entire length. In this study, high-resolution autonomous underwater vehicle (AUV) bathymetry is used to accurately map the extents of four historical fissure eruptions of the Juan de Fuca and Gorda ridges: on the North Gorda, North Cleft, and CoAxial ridge segments. The four mapped eruptions take the form of pillow mounds, which are similar in both lithology and dimension to hummocks on the Mid-Atlantic Ridge. Pillow mounds may be isolated, or coalesce to form composite mounds, aligned as ridges or as clustered groups. In three of the four mapped sites, the eruptions were discontinuous along their lengths, with pillow mounds and composite mounds commonly separated by areas of older seafloor. This style of discontinuous eruption is inconsistent with typical *en echelon* fissure eruptions and is probably due to a mildly overpressured, fingering dike intersecting the seafloor along parts of its length.

Components: 8,993 words, 7 figures, 1 table.

Keywords: mid-ocean ridge; Juan de Fuca Ridge; Gorda Ridge; pillow mound; hummock dike.

Index Terms: 3075 Submarine tectonics and volcanism: Marine Geology and Geophysics.

Received 24 November 2012; **Revised** 3 June 2013; **Accepted** 20 June 2013; **Published** 13 September 2013.

Yeo, I. A., D. A. Clague, J. F. Martin, J. B. Paduan, and D. W. Caress (2013), Preeruptive flow focussing in dikes feeding historical pillow ridges on the Juan de Fuca and Gorda Ridges, *Geochem. Geophys. Geosyst.*, *14*, 3586–3599, doi:10.1002/ggge.20210.

1. Introduction

[2] Volcanic eruptions on mid-ocean ridges typically take the form of fissure eruptions, which occur when a dike connects a magma chamber with the seafloor. In some scenarios, particularly when associated with low relief lava flows, fissures feeding lava flows can be observed on the seafloor [e.g., *Soule et al*., 2007], while in other areas they can be inferred by the presence of aligned volcanic constructions that bury them [e.g., *Smith et al*., 1995a]. Tensile cracking without an eruption produces fractures, which can be observed in most neovolcanic settings and are common at mid-ocean ridges.

[3] Fissure eruptions commonly begin by erupting lava along the entire length of the dike, but later focus down to several and, eventually, a single

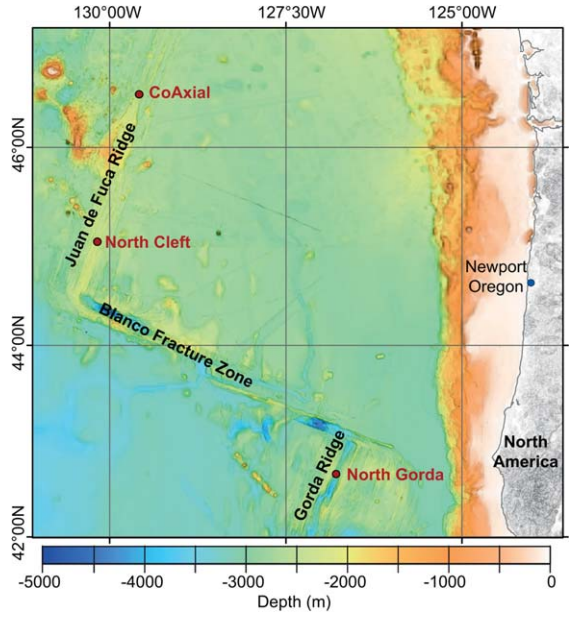

Figure 1. Locations of study areas on the Juan de Fuca and North Gorda Ridges. Seafloor bathymetry is taken from GMT satellite altimetry and the NGDC database.

point source. This flow focusing is a result of heat exchange between the magma and the walls of the dike. Cooling of sections of the flow within the dike creates temperature gradients, resulting in variations in viscosity and cross-sectional resistance to flow. The magma within the dike solidifies at different rates depending on numerous parameters, including the initial geometry of the fissure, mechanical effects, volatile exsolution, heterogeneities in the rock through which the fissure is propagating, and changes in the fissure dimensions [*Helfrich*, 1995; *Wylie et al*., 1999; *Bruce and Huppert*, 1989; *Delaney and Pollard*, 1982]. Sections of the dike solidifying while other sections remain open creates a flow focusing effect in which the magma flow becomes concentrated in a number of short sections of fissure as the eruption proceeds.

[4] Flow focusing is thought to be responsible for the common linear hummocky mounds observed at most slow-spreading and intermediate-spreading ridges [*Smith and Cann*, 1992], such as the Gorda and Juan de Fuca Ridges investigated in this paper (Figure 1). Volcanic mounds are called *hummocks* at slow-spreading mid-ocean ridges, and *pillow mounds* at intermediate-spreading ridges, and are one of the most common eruption styles observed at these spreading rates [*Chadwick et al*., 1991; *Chadwick and Embley*, 1994; *Fox et al*., 1992; *Briais et al*., 2000; *Smith and Cann*, 1990, 1992; *Smith et al*., 1995a, 1995b; *Yeo et al*., 2012; *Colman et al*., 2012]. Hummocks and pillow mounds are characterized by pillow lava flows, which pile on top of each other to form one or many cone-shaped or dome-shaped mounds, several hundred metres in diameter and tens of meters high. At intermediate-spreading ridges, the term "pillow mound" has been used to describe both single pillowed, hummock-like mounds as well as pillow mounds that have coalesced. In this study, we will distinguish between single and coalesced mounds by calling the first pillow mounds and the latter, which are commonly arranged in linear arrays, composite mounds (Figure 2).

[5] The North Gorda segment of the Gorda Ridge, and the CoAxial and North Cleft segments of the Juan de Fuca Ridge (Figure 1) are all intermediate rate spreading centers, with total spreading rates of 5.5, 5.5, and 6 cm/yr, respectively [*Riddihough*, 1984]. Eruptions occurred on the North Gorda segment in 1996, on the CoAxial segment both in 1993 and between 1982 and 1991, and on the North Cleft segment in1986.

[6] The North Gorda ridge in particular bears many similarities to the slow-spreading Mid-Atlantic ridge and is characterized by a deep, wide axial valley bounded by large normal faults. These ridge segments were selected for our high-resolution AUV surveys specifically because each had at least one known historical eruption that was mapped soon afterward (with preeruption/posteruption bathymetry with a resolution of ~30–50 m laterally and ~5 m vertically, and visual observations from camera tows, submersible and ROV studies). This early posteruptive characterization is critical to this study in that it guided identification of mounds formed during the historical eruptions from those that predate them.

[7] The historical eruptions at North Gorda, CoAxial, and North Cleft (Figures 3–5) were first identified from bathymetric and sidescan sonar studies and described as pillow ridges [*Chadwick et al*., 1998; *Chadwick and Embley*, 1994; *Embley et al*., 2000]. The other two historical eruptions on the Juan de Fuca Ridge occurred in 1998 and 2011 on Axial Seamount (46°55 N 130°00) [*Caress et al*., 2012; *Embley et al*., 1999; W. W. Chadwick et al., manuscript in preparation, 2013]. The 1998 eruption is a sheet flow and the 2011 eruption includes both sheet flows within the caldera and two pillow ridges down the south rift [*Caress et al*., 2012]. Recently developed methods of high-resolution bathymetry collection using an AUV [*Caress et al*., 2012; *Clague et al*., 2011] make it

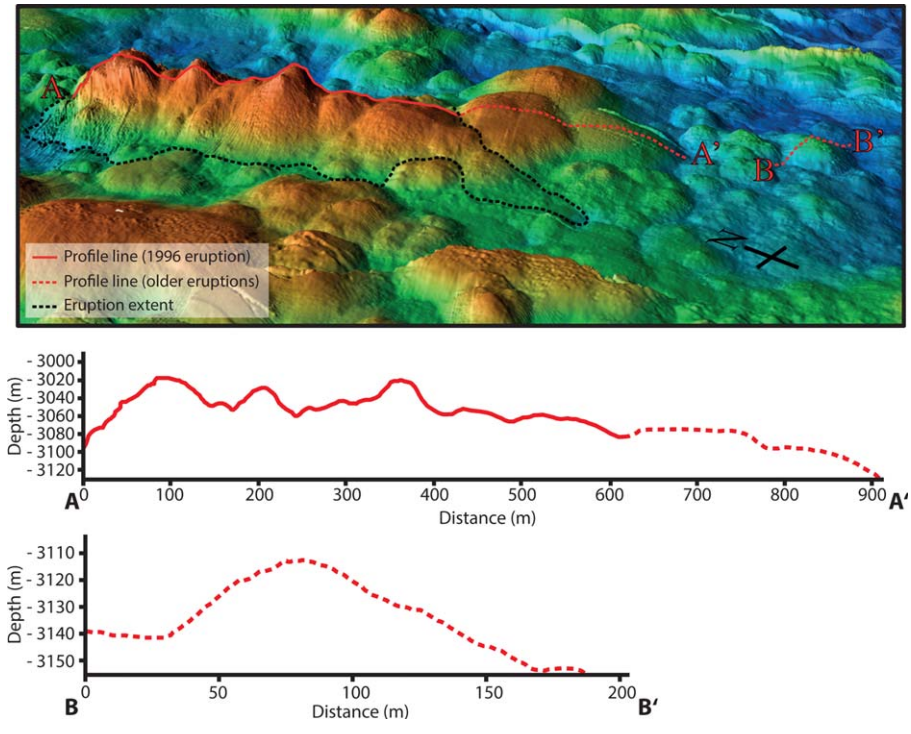

Figure 2. Examples of a composite and individual pillow mound in 3-D taken from the AUV bathymetry collected at North Gorda. Illuminated from the NW with no vertical exaggeration. The section of the composite mound covered by the solid line forms part of the 1996 eruption and is produced by a number of mounds growing on and against each other, while the southernmost two mounds covered by profile A and the individual mound are older. Profile tracks are indicated on the image. Field of view is approximately 1.2 km.

possible to image the flows in high resolution [e.g., *Rubin et al*., 2012], shedding light on how dikes propagate both laterally and vertically. The best way to determine the extent and volume of a seafloor eruption is to difference high-resolution preeruptive and posteruptive surveys, but this has only been accomplished for the 2011 flow at Axial Seamount [*Caress et al*., 2012]. However, a posteruptive survey, combined with visual observations can enable estimates of flow extents and volumes more accurately than is possible using lower resolution imaging techniques.

2. Materials and Methods

[8] High-resolution bathymetry was collected with the MBARI autonomous underwater vehicle (AUV) D. Allan B during a 2009 expedition on R/V Zephyr. The AUV surveyed from a 50 m altitude using a 200 kHz multibeam sonar [*Caress et al*., 2008]. The data were processed using MB-System [*Caress and Chaynes*, 1996], yielding bathymetric maps with ~1 m lateral resolution and ~0.1 m vertical precision. The full data processing workflow is described in *Clague et al*. [2011] and *Caress et al*. [2012]. The high-resolution bathymetry was colocated with the best available ship-based multibeam data, giving location accuracy on the order of 35 m.

[9] Video was recorded on high-resolution video cameras mounted on the MBARI remotely operated vehicles (ROVs) *Tiburon* (on Panasonic 3-chip pan and tilt color cameras recording to Digital Betacam™) and *Doc Ricketts* (using a ROS PT-25 pan and tilt HDTV) operated from the R/V *Western Flyer* on cruises in 2005, 2009, and 2011. The video was used to confirm flow morphologies, lava flow boundaries crossed by the dives, as well as flow superposition between units of different ages.

[10] Lava flow extents were identified using high-resolution bathymetry (predominantly from flow morphology changes and the degree of fracturing), video data and published glass and rock chemistry [*Davis and Clague*, 1987; *Davis et al*., 2008; *Rubin et al*., 1998] for samples from the area, plus additional and glass compositions for newly acquired samples. Where possible we also included observations from other published surveys carried out in the mapping areas. It is

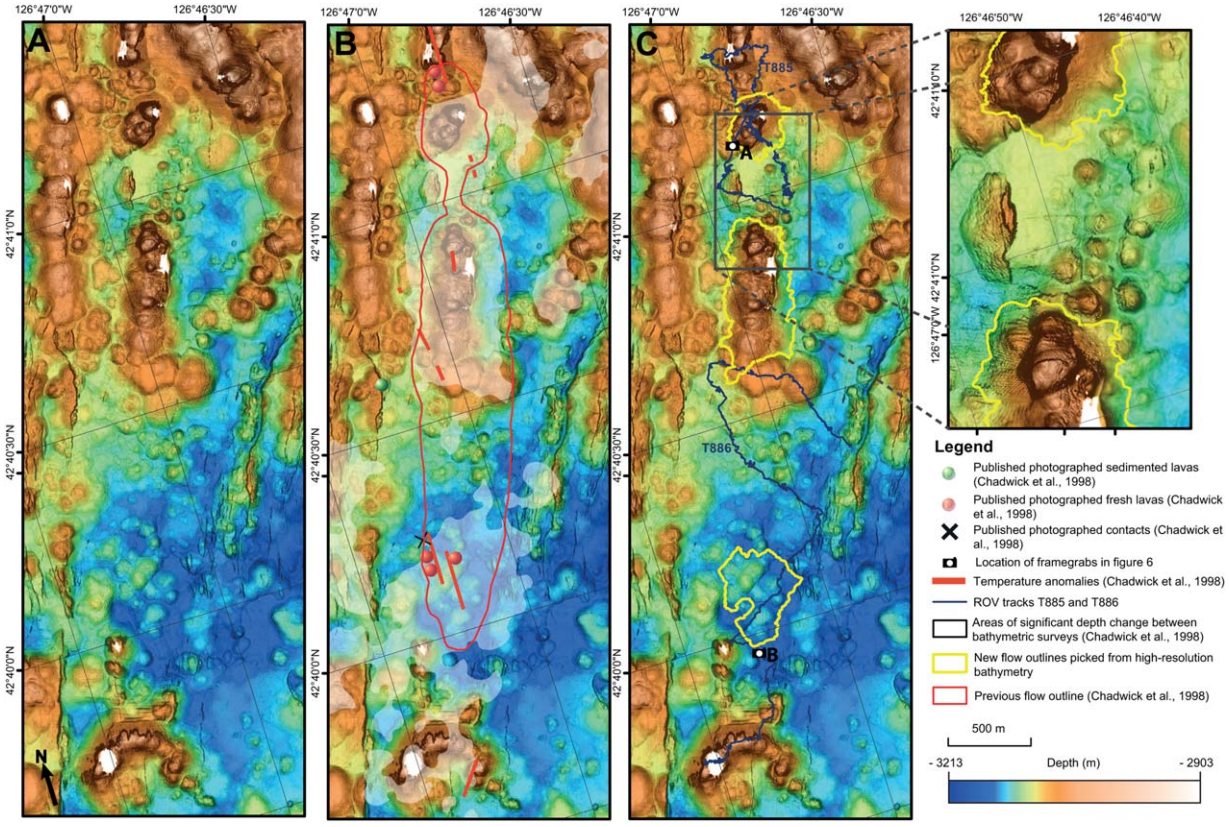

Figure 3. (a) AUV high-resolution (1 m) bathymetry of the 1996 eruption area on the North Gorda Ridge. The color ramp is histogram equalized to emphasize the highs and lows of the data set. (b) The same bathymetry showing the *Chadwick et al*. [1998] flow outline (red) from camera tows and areas of significant depth change between bathymetric surveys (shown in white). Thick red lines are temperature anomalies during camera tows. The locations of photographed lavas and contacts are published photos taken from extensive camera tow surveys. (c) The remapped eruption extents from this study. ROV dive tracks, where visual observations and samples were collected, are also shown, as are the locations of the video stills shown in Figure 6. Inset: Close-up of unfissured seafloor between two eruption locations.

possible that smaller areas of eruption (particularly if they did not produce a pillow mound) may have been missed from the maps, however the combination of visual observation and high-resolution bathymetric mapping, along with geochemical constrains, means we can be fairly confident that all the mounds included in each flow do belong to those eruptions. We can also be very certain that spatial separation between noncontiguous sections of contemporaneous lava flows exists between the flows at North Gorda and North Cleft, as these areas were covered by ROV dives and older sedimented flows were observed between eruption sites.

[11] Lava flow volumes were estimated using the high-resolution data sets for each of the surveys (gridded at either 1 m or 1.5 m) with lava flow shape files created using ESRI ArcGIS software. Volumes were calculated using the ArcGIS 10.0 Spatial Analyst Cut-Fill tool. The high-resolution AUV bathymetry grids provided accurate posteruption surfaces, but, since high-resolution bathymetry was not collected beforehand, preeruption surfaces were estimated using the surrounding posteruption bathymetry. Detailed outlines were drawn around each recently erupted pillow mound, and posteruption depth values were extracted for each vertex along this outline. Natural neighbor interpolation between these points was then used to create an artificial preeruption surface beneath each pillow mound. The natural neighbor interpolation technique works with irregularly distributed points, utilizes only the closest input points, and creates a smooth surface that passes directly through the input points. This artificially generated preeruption surface was then subtracted from the posteruption 1 m resolution bathymetry to provide a volume estimate of each pillow mound. When

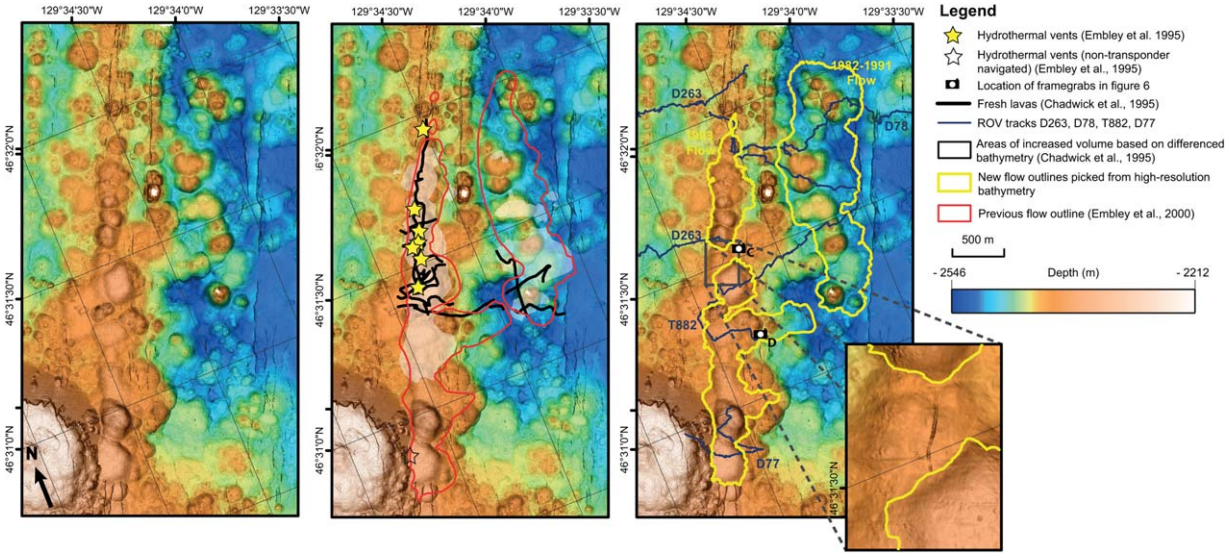

Figure 4. (a) AUV high-resolution (1 m) bathymetry of the 1993 and 1982–1991 eruption areas on the CoAxial segment of the Juan de Fuca ridge. The color ramp is histogram equalized to emphasize the highs and lows of the data set. (b) The same bathymetry showing the Embley et al. [2000] flow outlines (red) from visual observations, sidescan data, and areas of significant depth change between bathymetric surveys (shown in white), along with mapped areas of fresh lavas and hydrothermalism. (c) The remapped lava flow extents for each eruption from this study. ROV dive tracks, where visual observations and samples were collected, are also shown, as are the locations of the video stills shown in Figure 6. Inset: Close-up of a fissure between two composite mounds from the 199s flow. Fresh lavas were observed in this area but the fracture can clearly be seen being truncated to the north and south by younger lava flows.

applied to the 2011 eruption at Axial Volcano [*Caress et al*., 2012], this method yielded results with errors between 30 and 60% of the actual eruption volume. We can therefore say that flow volume estimations are known to better than a factor of two. Preeruptive ship bathymetry was not used for volume calculations as it is low resolution and was collected before GPS ship navigation, making comparison of the data sets problematic.

[12] All the historical lava flows discussed in this paper comprise one or more composite mound, each made up of several to tens of individual pillow mounds. Pillow mounds were identified as any rounded volcanic mounds, with heights >5 m, following the definition of *Yeo et al*. [2012] for hummocks on the Mid-Atlantic Ridge. The average height and diameter of pillow mounds from each site were measured. Pillow mounds were picked as a circle, which approximated its base, and a point representing its shallowest point. Pillow mound dimensions were measured using ArcGIS software, their spacing was measured base to base. Mound heights were approximated following the method of *Yeo et al*. [2012], by averaging the depths of areas of flat seafloor around the circle used to define each pillow mound's base, and subtracting these from the peak depth. The estimated preeruption surface used for volume approximations was not used to measure mound heights as it produced artificially large heights for mounds that had built on top of one another.

3. Observations

[13] All four historical eruptions (North Gorda 1996, CoAxial 1993 and 1982–1991, and North Cleft 1986) were mapped in the new 1 m resolution bathymetry (Figures 3–5), and take the form of pillow mound eruptions, which commonly coalesced to form composite mounds. The 1996 North Gorda eruption mounds extend for 2.44 km on a bearing of ~015°, the 1993 CoAxial lava flow outcrops for 2.49 km on a bearing of ~020°, the 1982–1991 CoAxial flow for 1.62 km on a bearing of ~20°, and the North Cleft 1986 eruption for 17 km on a bearing of ~017°.

3.1. North Gorda

[14] The 1996 North Gorda eruption (Figure 3) lies within a 0.8–1.5 km wide inner valley, bounded to the east and west by 20–40 m throw,

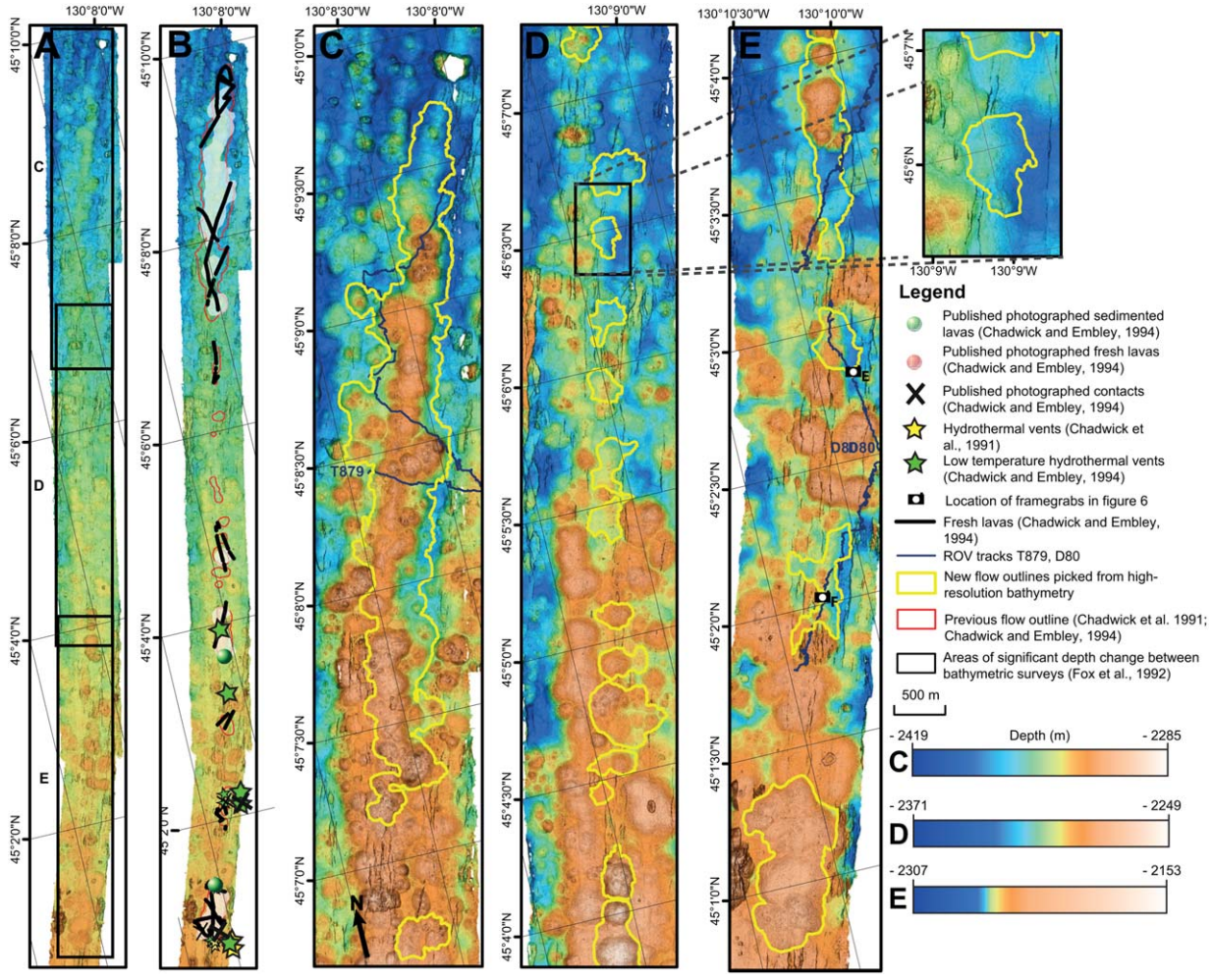

Figure 5. (a) AUV high-resolution (1 m) bathymetry of the 1986 eruption area on the North Cleft segment of the Juan de Fuca ridge. (b) The same bathymetry showing the *Chadwick and Embley* [1994] estimation of eruption extents, and locations of fresh lavas, hydrothermalism, visual observations and areas of significant depth change between bathymetric surveys. The locations of photographed lavas and contacts are published photos taken from extensive camera tow surveys. (c–e) Close-up of the same bathymetry showing the remapped lava flow extents from this study. Color ramps are histogram equalized to emphasize the highs and lows of each panel. ROV dive tracks, where visual observations and samples were collected, are also shown, as are the locations of the video stills shown in Figure 6. Inset: Close-up of two separate eruption sites showing fissuring between them.

inward facing normal faults (only a small section of the eastern bounding fault is shown in Figure 3). The bounding fault scarps are discontinuous and appear to have been overtopped by younger lava flows in several places, for example at 42°40′25 N on the western scarp. The inner valley floor is characterized by a number of relatively unfractured, young looking pillow mound ridges composed of fresh basalts (Figure 6a), as well as some very fractured pillow mound ridges. The contacts were generally fairly clear in the ROV observations (e.g., Figure 6b) but were sometimes buried by talus. The predominant orientation of groups of pillow mounds is not always aligned with the strike of the ridge with some, such as the ridge centered on 42°40′45 N 126°46′33 W, angled >25° from the segment trend. Other pillow mounds form irregular-shaped agglomerations (which have no alignment) rather than ridges. Almost all the pillow constructions associated with this eruption, as well as with the other three historical eruptions described in the following sections, are built of coalesced, nearly circular pillow mound building blocks, similar to those described on the slow-spreading Mid-Atlantic Ridge [*Smith and Cann*, 1990; *Yeo et al.*, 2012].

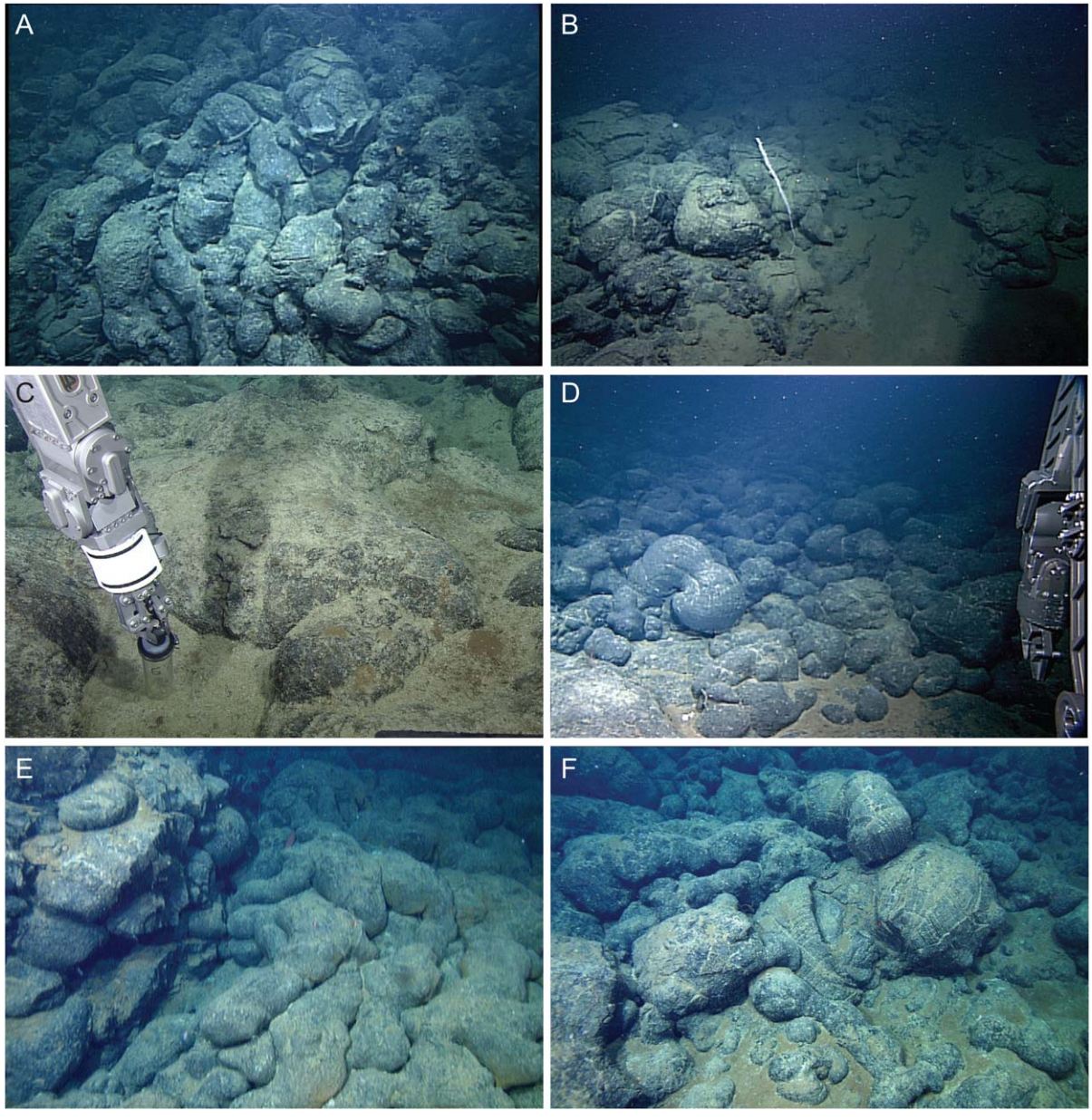

Figure 6. (A and B) Framegrabs collected in 2005 with ROV *Tiburon* from the 1996 North Gorda pillow mound; the image locations are indicated on Figure 3. Figure 6A shows the bulbous and elongate pillows that construct the steep mounds and the general lack of sediment 9 years posteruption. Figure 6B shows the contact between the 1996 lava (left) and an older, more heavily sediment covered flow (right). The white bamboo coral is at the contact. (C and D) Framegrabs collected in 2011 and 2005 using ROVs *Doc Ricketts* and *Tiburon*, respectively, from the vicinity of the 1993 CoAxial pillow mound; the image locations are indicated on Figure 4. Figure 6C shows a pushcore collection of sediment accumulated on pre-1993 pillow lava just SE of the offset between two *en echelon* fissures that fed the 1993 pillow ridge. Figure 6D shows a contact between bulbous pillow lavas of the 1993 flow and an apparently more heavily sedimented, lower-relief pillow flow in the foreground. (E and F) Framegrabs collected in 2009 by ROV *Doc Ricketts* at the 1986 North Cleft pillow mounds; the image locations are shown on Figure 5. Figure 6E shows 1986 elongate pillow lavas (right) ramped against a fault scarp of older lavas. Figure 6F shows the 1986 bulbous pillow lavas (upper left) on top of older, more heavily sediment-covered, smaller pillows. Sediment accumulation and the dulling of glassy lava surfaces in the 23 years since flow emplacement makes it much less obvious where the contacts are located. All images show a field of view approximately 4–5 m across except Figure 6C, which is about 1–2 m wide.

Table 1. Pillow Mound and Flow Dimensions for All Four Historical Eruptions[a]

Eruption	Pillow Mounds	Average Diameter (m)	Average Height (m)	Height: Diameter Ratio	Area (km^2)	Volume (km^3)	Average Thickness (m)	Maximum Thickness (m)
North Gorda 1996	29	79	29	1:3.1	0.31	0.007	23	114
CoAxial 1993	38	85	16	1:5.3	0.61	0.009	25	64
CoAxial 1982–1991	65	75	21	1:3.7	0.64	0.019	29	101
North Cleft 1986	130	90	12	1:7.4	3.83	0.048	13	65

[a]Diameters, heights, and thicknesses are given as averages for the entire eruption.

[15] The 1996 North Gorda eruption produced 29 pillow mounds forming three distinct composite mounds. Individual mounds have an average diameter of 79 m and average heights of 25 m, giving diameter:height ratios of 1:3.1 (Table 1). *Chadwick et al*. [1998] found up to 75 m of depth change between preeruption and posteruption ship based multibeam surveys at the northern end of the site, which is slightly less that the maximum measured increase of 114 m measured using the interpolated base surfaces (Table 1). At its northern end, most of the pillow mounds are aligned along the presumed feeder fissure; however, the southernmost section of extrusion has produced a more spread out area of pillow mound terrain, which is in places three mounds across. This map is considerably different to that in *Chadwick et al*. [1998], although the new outlines are consistent with the observations from these previous studies. They differ because new observations from the Tiburon ROV dives between the mounds revealed no new lavas had been erupted there.

3.2. CoAxial

[16] The CoAxial segment between 46°30′N and 46°33′N has been the site of two historical eruptions, in 1993 and between 1982 and 1991, both of which lie within a 2.8 km wide inner valley (Figure 4). The valley is bounded to the east and west by 30–50 m throw, inward facing normal faults (not shown). Around two thirds of the inner valley is characterized by typical hummocky seafloor, while the easternmost third (up to the base of the eastern valley bounding faults) is covered by an extensive sheet flow. The south-western section of the survey area is dominated by a large (1.1 km diameter, 150 m high), flat-topped seamount. Both historical flows occurred in the hummocky area; the 1982–1991 eruption occurred on its eastern edge (roughly down the center of the axial valley) and the 1993 eruption occurred in the center of the hummocky area, on the west of the valley center. The earthquake swarm associated with the 1993 eruption migrated northward, initially overshooting the eruption site and then focussing on it after 3 days of activity, suggesting the magma source was south of the eruption [*Dziak et al*., 1995]. This eruption produced graben structures to the outside northern and southern extents of lava effusion, which have been linked to the intrusion of the feeder dike at shallow depths. Grabens further south are also thought to be associated with the same dike [*Chadwick and Embley*, 1998].

[17] The 1993 eruption at CoAxial produced 38 pillow mounds, which take the form of two large composite mounds (examples of older lava in Figure 6C) and one discrete pillow mound. This is just connected to the composite mound to the south. The discrete mound is offset slightly to the east of the southern composite mound, although this may be an effect of slope. A possible contact can be seen at the top of the northern most "tongue" (Figure 6D), however seafloor video footage acquired just after the eruption suggests that this section is still part of the 1993 flow (W.W. Chadwick, personal communication, 2013). Pillow mounds have an average diameter of 85 m and average heights of 16 m (averaged height of basal contour method). Maximum measured increases from the interpolated base surfaces were 64 m, slightly more than the depth change of 29 m [*Chadwick et al*., 1995] between preeruption and posteruption ship-based multibeam surveys. Pillow mound diameter to height ratios were 1:5.3 (Table 1).

[18] The other historical CoAxial eruption, which occurred between 1982 and 1991, produced 65 pillow mounds, forming a single, large composite mound. The individual mounds have an average diameter of 75 m, average heights of 21 m, and diameter to height ratios of 1:3.7 (Table 1), similar to both the 1993 eruption at CoAxial and the 1996 eruption at North Gorda. *Chadwick et al*. [1995] found depth changes of up to 37 m associated with this flow, compared with maximum increases of 101 m measured from the interpolated base surfaces (Table 1).

3.3. North Cleft

[19] The overlap between the northern Cleft segment and the Vance segment (Figure 5), where the 1986 eruption occurred, is not technically a "valley" setting. However, the pillow mounds are localized predominantly in the center of a 1 km wide graben bounded by <20 m throw inward facing normal faults. The pillow mounds are less clearly defined than on the other ridge segments, often occurring as a single broad high with several <5 m high peaks, and in places forming flatter, more irregular-shaped areas of fresh lavas, although again contacts were usually fairly clear (Figures 6e and 6f). South of the eruption site the entire valley is covered by extensive sheet flows (not shown), which are young but apparently not part of the 1986 eruption that produced the mounds [*Chadwick et al*., 1999; *Embley et al*., 1991; *Embley and Chadwick*, 1994]. The 1986 eruption occurred in the middle of the hummocky zone, roughly in the center of the graben. The eruption here is also discontinuous, with areas of fractured, older seafloor separating the unfractured mounds.

[20] The 1986 eruption at North Cleft produced 130 pillow mounds, many of which coalesced. We find 17 separate eruption sites along the fissure, although not all are characterized by pillow mounds, and noticeably fewer pillow mounds occur at the southern end of the eruption than at the northern end, where they coalesce to form a large composite mound. This is compared to nine discrete mounds mapped by *Chadwick et al*. [1991] and 13 discrete mounds mapped by *Chadwick and Embley* [1994]. At its northern end, 91 of the pillow mounds form a 5 km long composite mound that contains ~75% of all the erupted material. Of the other eruption sites, pillow mounds can be identified on seven, while the others consist of smooth, flat, or undulating lava flows. It has been suggested, based on diverse compositions of samples collected that this northernmost mound could be a composite, multieruption edifice and that the similar diversity observed in samples from the separate mounds suggests diking from a compositionally heterogeneous magma chamber [*Rubin et al*., 2001]. We cannot rule this out, however where covered by dive T879 the lavas appeared fresh and unsedimented and therefore these eruptions must have occurred closely spaced in time. This is supported by the lack of fissuring or faulting observed along the large mound and therefore we map this mound as a single edifice.

[21] The pillow mounds have an average diameter of 90 m and average heights of 12 m, yielding diameter to height ratios of 1:7.4 (Table 1). Our maximum measured thickness is 65 m (Table 1), compared to *Fox et al*. [1992], who found depth changes up to 45 m at the northern end of the eruption. The pillow mounds at North Cleft are noticeably shorter than those observed on the other segments, and also have the largest average diameter (and corresponding diameter to height ratios).

3.4. Flow Areas and Volumes

[22] The new high-resolution bathymetric maps and new ROV observations combined with the observations from previous studies have made it possible to relatively accurately identify flow boundaries on the seafloor for these three areas. In particular, North Gorda was previously mapped as a single coalesced ridge (Figure 3) [*Chadwick et al*., 1998] based on differenced preeruption and posteruption bathymetric surveys and visual observations of the seafloor. The high-resolution maps have made different interpretation possible, in which flows along this section are highly discontinuous. *Chadwick and Embley* [1994] identified 13 individual pillowed mounds at North Cleft and we refine the mapping of these mounds, and identify an additional four composite mounds, bringing the total number of eruptive mounds to 17 (Figure 5). Some of these mounds were originally mapped as one single mound, but the high-resolution bathymetry reveals they are separated by older, fractured seafloor. The North Gorda, 1993 CoAxial and 1982–1991 CoAxial eruptions cover similar areas (0.31, 0.62, and 0.65 km^2, respectively) (Table 1). At CoAxial, these values are both similar to the values estimated from previous studies, however at North Gorda the new area is less than half that originally estimated [*Chadwick et al*., 1998]. The 1986 North Cleft mounds, in contrast, covered an area of 3.8 km^2, noticeably greater than the other three eruptions, and slightly larger than the previous estimate of 2.8 km^2 [*Chadwick et al*., 1998].

[23] Calculating flow volumes is uncertain without high-resolution bathymetry before and after the eruption [*Caress et al*., 2012], however we are able to estimate flow volumes using the interpolated natural neighbor surfaces. This method gives volumes of 0.007 km^3 (with an average thickness of 23 m) for North Gorda; 0.009 km^3 (with an average thickness of 15 m) for the 1993, and 0.019 km^3 (with an average thickness of 29 m) for the 1982–1991 eruptions at CoAxial; and 0.048 km^3

(with an average thickness of 13 m) at North Cleft (Table 1). These estimates are similar to previously published volumes for the 1993 CoAxial and the North Cleft flows, but the North Gorda 1996 eruption volume is noticeable smaller than original estimate, almost certainly due to the smaller area mapped, while the new 1982–1991 CoAxial estimate is somewhat larger than the original, probably due to a greater average thickness across the flow [*Chadwick et al*., 1998].

3.5. Mound Connectivity

[24] Distinct centers of eruptive activity within the same eruption ranged from 1 (Coaxial 1982–1991) to 17 (1986 North Cleft). The composite pillow mounds formed during the 1996 North Gorda, 1993 CoAxial, and 1986 North Cleft eruptions are unconnected to each other (Figures 3 and 5). Composite mounds at North Gorda show no fracturing between mounds (Figure 3 inset as opposed to Figure 5 inset), and there is only a small amount of fracturing visible at CoAxial (Figure 4 inset), although grabens have been documented north and south of the CoAxial 1993 eruption [*Chadwick and Embley*, 1998]. Grabens or fractures might be expected if the fissure eruption intersected the seafloor along the entire length of the dike trace, or if the top of the dike closely approached the seafloor [*Chadwick and Embley*, 1998; *Rubin*, 1992]. Fairly extensive fracturing is observed between composite mounds at North Cleft (Figure 5).

4 Discussion

4.1. Discontinuous Eruptions

[25] The pillow ridges produced during three of the four historical eruptions are discontinuous. Discontinuous eruptions had been observed at North Cleft and other parts of the Juan de Fuca ridge [*Caress et al*., 2012; *Embley et al*., 2000; *Chadwick et al*., 2001] and at the Galapagos Spreading Center [*Colman et al*., 2012], suggesting that they are fairly common. Our mapping reveals a distinct separation between eruptive centers in which no fresh lavas are observed. Additionally, at North Gorda we observe no fracturing of the seafloor between the fresh pillow mounds, which, had there been fractures, would be indicative of a dike at shallow depth below the surface. This suggests flow localization is occurring before the dike reaches the surface, and may occur at substantial depths. This effect, known as "dike fingering," has been recognized for igneous intrusions occurring under high confining pressure on land [*Pollard et al*., 1975; *Rubin*, 1993] and in analog models [*Helfrich*, 1995].

[26] Unlike *en echelon* fissure eruptions observed on land [*Mattsson and Höskuldsson*, 2011; *Moore and Krivoy*, 1964; *Moore et al*., 1980; *Parcheta et al*., 2012; *Thordarson and Self*, 1993] and on some mid-ocean ridges [*Caress et al*., 2012; *Crane and Ballard*, 1981; *Soule et al*., 2009], the mounds in the observed historical eruptions are not always offset to one side, instead lining up with each other along what is presumably the strike of the underlying dike. Additionally, unlike en echelon situations, the eruptive fissures do not overlap at their ends, and are often separated by several hundred metres of unfractured seafloor. This outcrop pattern is markedly different to those produced by en echelon fissure eruptions (which are caused by discordance of dike and near-surface principle stress orientations [*Pollard et al*., 1982; *Ziv and Rubin*, 2000; *Rubin*, 1995]) and instead appears to reflect an irregular (fingered) dike propagation front. Fingering dike fronts may be the result of heterogeneities in the rock being intruded, or as a result of shear failures along the dike front, but have also been modeled in homogenous situations [*Helfrich*, 1995; *Touvet et al*., 2011; *Pollard et al*., 1975; *Rubin*, 1993; *Delaney and Pollard*, 1981].

[27] In this scenario, one or more sections of the dike will intersect the seafloor first, resulting in a change in the pressure within the dike. The dike will continue to propagate until the pressure within the propagating tip is no longer high enough to crack rock. If this happens before the entire dike intersects the seafloor as a single fissure then discrete sections of the dike will erupt, rather than the whole length. This process would explain the alignment of the eruptive fissures as well as the variable lengths of the eruptive gaps between them. It also suggests that the dikes are only mildly overpressured, as intersection of the seafloor along only some of their length reduced the pressure in the dike tip enough to halt its propagation. This would also be consistent with analog experiments that show that pillow flow morphology is the product of eruptions with a relatively low effusion rate [*Griffiths and Fink*, 1992; *Gregg and Fink*, 1995]. The discontinuous and variable nature of the grabens observed by *Chadwick and Embley* [1998] would not be inconsistent with the fingering dike model as they could also indicate variations in the depth and width of the dike beneath the surface.

[28] Emplacement of mounds may be simultaneous, sequential, or discrete in time. Simultaneous emplacement would be consistent with a vertical dike tapping an underlying magma source, while sequential emplacement could be consistent with a dike propagating away from a magma source, which perhaps was the case for the earthquake swarm observed for the CoAxial 1993 eruption [*Dziak et al*., 1995]. Evidence from a larger eruption at Veidivötn in Iceland displays similar separate segments, separated by areas with no extrusive volcanic eruption [*Larsen*, 1984]. These segments appear to have been active at the same time and are thought to be produced by the vertical feeding of magma to the individual structures from an underlying magma source [*Zellmer et al*., 2008]. Similar eruptions, consisting of discrete mound like structures have also been documented at Krafla [e.g., *Buck et al*., 2006] and in Iceland's western volcanic zone [e.g., *Sinton et al*., 2005].

[29] The existence of larger elongate composite mounds suggests that some dikes are wide enough or have high enough flow rates to develop a stable flow to the surface along parts of their length (as this section of the dike stays active longer than the surrounding sections). The much larger volume of these mounds also indicates that they may erupt for longer than the smaller mounds or have higher effusion rates, although any substantial increase in effusion rate would favor the production of lobate over pillow flows, leading to the production of flatter pillow mounds. This is not observed on the Juan de Fuca or North Gorda Ridges, although many mound structures on the Galapagos Spreading Centre are flat topped [*Colman et al*., 2012]. This suggests that as the eruption continues, the smaller dike fingers, which originally reached the surface and fed the smaller composite mounds, also solidify. This leads to further point focusing to just one or two robust dike fingers with a width or magma flux great enough for them to remain active for longer periods.

4.2. Pillow Mounds

[30] The pillow mounds observed in these studies are similar to those measured using similar resolution data for hummocks from 45°N on the Mid-Atlantic Ridge [*Yeo et al*., 2012]. Both are primarily composed of pillow lavas, although those covered in this study show fewer collapses than documented at the Mid-Atlantic Ridge—possibly because they are younger [*Yeo et al*., 2012]. The pillow mounds also have similar dimensions to the Mid-Atlantic Ridge hummocks (Figure 7). Similar, 10–20 m high, approximately 200 m diameter, aligned structures have also been observed less commonly on the superfast spreading East Pacific Rise [*White et al*., 2000; *Sinton et al*., 2002].

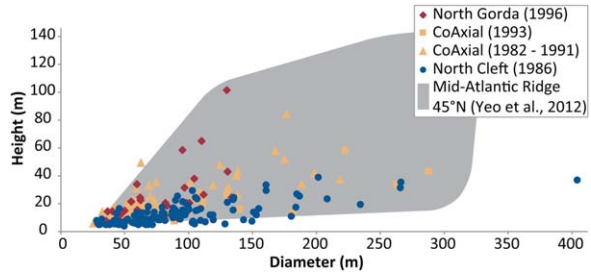

Figure 7. Pillow mound dimensions for all four historical eruptions plotted as diameter against height. The gray zone represents the spread of diameter against height data for hummocks measured on the Mid-Atlantic Ridge at 45°N from *Yeo et al*. [2012] using the same method. In general, the pillow mounds at North Cleft are flatter than those at North Gorda or Coaxial, particularly where diameters exceed 100 m. Larger basal diameters are also more common at North Cleft than at CoAxial and especially North Gorda, where no basal diameters exceed 150 m. Almost all the data for the historical eruptions lie within the envelope for hummocks measured at the Mid-Atlantic Ridge.

[31] The North Cleft segment displays slightly higher typical height:diameter ratios than at the North Gorda or CoAxial segments, particularly at diameters >50 m (Figure 7). These flatter mounds are likely to be the result of longer run out flows, and at the Mid-Atlantic Ridge similar, flatter hummocks corresponded with lobate lava flows at summits rather than the more common pillowed summits. Run out of flows is linked to lava morphology and has been linked to effusion rate, lava rheology and underlying slope. Longer run out flows tend to be lobate or sheet flows and their production is favored by higher effusion rates, steeper underlying slopes and lower lava viscosities [*Griffiths and Fink*, 1992; *Gregg and Fink*, 1995]. There is no relationship between aspect ratio and mound spacing, suggesting that these factors do not control the spacing of the mounds themselves.

[32] The distribution of the mounds on the seafloor is also interesting. Despite the fact that the eruptions are almost certainly fed by dikes, the arrangement of mounds is not always strictly linear. This is particularly well demonstrated by the 1982–1991 CoAxial flow, where it is very hard to pick where the feeder dike lies beneath the

eruption, and by the 1996 North Gorda eruption, where the clearly focussed feeder dike can be easily picked in the northern two sites, but is almost impossible to pick at the southernmost one. For these off-strike mounds to be fed directly by the dike would require large deviations in its strike and position in the shallow subsurface. Alternatively such mounds may be fed by the exploitation of preexisting weaknesses in the heterogeneously fissured and fractured seafloor, or by the lateral transport of magma through or beneath the on-strike mounds.

4.3. Eruption Rates

[33] The 1996 North Gorda and the 1993 CoAxial eruptions were detected by the U.S. Navy's SOSUS (SOund SUrveillance System) [*Fox and Dziak*, 1998; *Dziak et al*., 1995] network producing durations of seismic disturbance of 523 and 453 h, respectively. Assuming the eruption was occurring for the entire duration of the seismic activity, these durations combined with the eruption volume estimates give eruption rates of 320,000 m^3 per day (13,000 m^3 per hour) for North Gorda and 475,000 m^3 per day (20,000 m^3 per hour) for CoAxial. It should be noted however that the duration of seismicity is not necessarily the same as the duration of the eruption, seismicity may go on for longer than the eruption [e.g., *Fox et al*., 2001], or alternatively an eruption could continue at a low effusion rate without producing high level seismicity. Therefore, these values are only estimates. Additionally, the fissure is unlikely to erupt at a constant rate for the entire eruption duration and therefore we would expect effusion rate to vary above and below these estimates.

5. Conclusions

[34] Eruptions at intermediate-spreading rate ridges often take the form of pillow mound eruptions, which are commonly discontinuous. The 1996 North Gorda, 1993 CoAxial, and the 1986 North Cleft eruptions are composed of such discontinuous pillow mounds, which are separated by older seafloor that may or may not be fissured or fractured. Pillow mounds have similar dimensions and are probably formed the same way as hummocks at slow-spreading mid-ocean ridges. The pillow mounds at North Cleft are slightly flatter than those observed at the other two segments, although they are still within the size range of those observed at the Mid-Atlantic Ridge.

[35] A number of small, discrete, or composite pillow mounds can be formed during a single eruption, with no erupted products or surface fractures between them. In places these mounds are aligned and probably represent the irregular propagation front of a mildly overpressured dike intersecting the seafloor at discrete locations. Pillow mounds may be emplaced sequentially or at the same time.

[36] Estimated flow volumes for the four historical eruptions range from 0.007 to 0.048 km^3, with coverage areas from 0.31 to 3.83 km^2. These estimates are similar to those estimated by differencing preeruptive and posteruptive bathymetry, however these new maps of eruption extents are more detailed and more accurate than were previously possible. High-resolution bathymetry sheds new light on the morphology of historically erupted pillow mounds and their architecture and has implications for the emplacement of submarine lava erupted at a relatively low-effusion rate.

Acknowledgments

[37] We thank Bill Chadwick and Ken Rubin for detailed reviews and information, which have greatly improved the manuscript. AUV surveys, ROV dives, and salaries for DAC, JBP, JFM, and DWC were supported by the Monterey Bay Aquarium Research Institute (MBARI), through grants from the David and Lucile Packard Foundation. IAY was supported by an internship at MBARI during summer 2010. We thank the shipboard scientific party, officers, crew and technicians of R/V *Western Flyer* and R/V *Zephyr* for their dedication and professionalism in assisting in the data acquisition. We also thank Roger Searle for advice and guidance.

References

Briais, A., H. Sloan, L. M. Parson, and B. J. Murton (2000), Accretionary processes in the axial valley of the Mid-Atlantic Ridge 27°N–30°N from TOBI side-scan sonar images, *Mar. Geophys. Res.*, *21*, 87–119.

Bruce, P. M., and H. E. Huppert (1989), Thermal control of basaltic fissure eruptions, *Nature*, *342*, 665–667.

Buck, W. R., P. Einarsson, and B. Brandsdóttir (2006), Tectonic stress and magma chamber size as controls on dike propagation: Constraints from the 1975–1984 Krafla rifting episode, *J. Geophys. Res.*, *111*, B12404, doi:10.1029/2005JB003879.

Caress, D. W., and D. N. Chaynes (1996), Improved processing of hydrosweep DS multibeam data on the R/V maurice ewing, *Mar. Geophys. Res.*, *18*, 631–650.

Caress, D. W., H. Thomas, W. J. Kirkwood, R. Mcewen, R. Henthorn, D. A. Clague, C. K. Paull, J. Paduan, and K. L. Maier (2008), High-resolution multibeam, sidescan, and

subbottom surveys using the MBARI AUV D Allan B., in *Marine Habitat Mapping Technology for Alaska*, edited by J. R. Reynolds, and H.G. Greene, Alaska Sea Grant, University of Alaska Fairbanks. doi:10.4027/mhmta.2008.04, pp. 47–69.

Caress, D. W., D. A. Clague, J. B. Paduan, J. F. Martin, B. M. Dreyer, W. W. Chadwick, A. Denny, and D. S. Kelley (2012), Repeat bathymetric surveys at 1-metre resolution of lava flows erupted at Axial Seamount in April 2011, *Nat. Geosci.*, *5*(7), 483–488, doi:10.1038/ngeo1496.

Chadwick, W., and R. W. Embley (1998), Graben formation associated with recent dike intrusions and volcanic eruptions on the mid-ocean ridge, *J. Geophys. Res.*, *103*(B5), 9807–9825.

Chadwick, W. W., and R.W. Embley (1994), Lava flows from a mid-1980s submarine eruption on the Cleft segment, Juan de Fuca Ridge, *J. Geophys. Res.*, *99*(B3), 4761–4776.

Chadwick, W. W., R. W. Embley, and C. G. Fox (1991), Evidence for volcanic eruption on the southern Juan de Fuca ridge between 1981 and 1987, *Nature*, *350*, 416–418.

Chadwick, W. W., R. W. Embley, and G. Fox (1995), SeaBeam depth changes associated with recent lava flows, CoAxial segment, Juan de Fuca Ridge: Evidence for multiple eruptions between 1981–1993, *Geophys. Res. Lett.*, *22*(2), 167–170.

Chadwick, W. W., R. W. Embley, and T. M. Shank (1998), The 1996 Gorda Ridge eruption: Geologic mapping, sidescan sonar, and seabeam comparison results, *Deep Sea Res., Part II*, *45*, 2547–2569.

Chadwick, W. W., R. W. Embley, and T. K. P. Gregg (1999), Submarine lineated sheet flows: A unique lava morphology formed on subsiding lava ponds, *Bull. Volcanol.*, *61*, 194–206.

Chadwick, W. W., D. S. Scheirer, R.W. Embley, and H.P. Johnson (2001), High-resolution bathymetric surveys using scanning sonars: Lava flow morphology, hydrothermal vents, and geologic structure at recent eruption sites on the Juan de Fuca Ridge, *J. Geophys. Res.*, *106*(B8), 16,075–16,099.

Clague, D. A., J. B. Paduan, D. W. Caress, H. Thomas, W. W. Chadwick, and S. G. Merle (2011), Volcanic morphology of West Mata Volcano, NE Lau Basin, based on high-resolution bathymetry and depth changes, *Geochem. Geophys. Geosyst.*, *12*, QOAF03, doi:10.1029/2011GC003791.

Colman, A., et al. (2012), Effects of variable magma supply on mid-ocean ridge eruptions: Constraints from mapped lava flow fields along the Galápagos Spreading Center, *Geochem. Geophys. Geosyst. 13*, Q08014, doi:10.1029/2012GC004163.

Crane, K., and R. D. Ballard (1981), Volcanics and structure of the FAMOUS Narrowgate Rift: Evidence for cyclic evolution: AMAR 1, *J. Geophys. Res.*, *86*(B6), 5112–5124.

Davis, A. S., and D. A. Clague (1987), Geochemistry, mineralogy, and petrogenesis of basalt from the Gorda Ridge, *J. Geophys. Res.*, *92*(B10), 10,467–10,483, doi:10.1029/JB092iB10p10467.

Davis, A. S., D. A. Clague, B. L. Cousens, R. Keaten, and J. B. Paduan (2008), Geochemistry, mineralogy, and petrogenesis of basalt from the Gorda Ridge, *Geochem. Geophys. Geosyst. 9*, Q04004, doi:10.1029/2007GC001775.

Delaney, P. T., and D. D. Pollard (1981), Deformation of host rocks and flow of magma during growth of minette dikes and breccia-bearing intrusions near ship rock, New Mexico, U.S. Geol. Surv. Prof. Pap., 1201.

Delaney, P. T., and D. D. Pollard (1982), Solidification of basaltic magma in a dike, *Am. J. Sci.*, *282*, 856–885.

Dziak, R. P., G. Fox, and A. E. Schreiner (1995), The June-July 1993 seismo-acoustic event at CoAxial segment, Juan de Fuca Ridge: Evidence for a lateral dike injection, *Geophys. Res. Lett.*, *22*(2), 135–138.

Embley, R. W., and W. W. Chadwick (1994), Volcanic and hydrothermal processes associated with a recent phase of seafloor spreading at the northern Cleft segment: Juan de Fuca Ridge, *J. Geophys. Res.*, *99*(B3), 4741–4760.

Embley, R. W., W. W. Chadwick, M. R. Perfit, and E. T. Baker (1991), Geology of the northern Cleft segment, Juan de Fuca Ridge: Recent lava flows, sea-floor spreading, and the formation of megaplumes, *Geology*, *19*, 771–775, doi:10.1130/0091–7613(1991)019<0771.

Embley, R. W., W. W. Chadwick, D. A. Clague, and D. Stakes (1999), 1998 Eruption of axial volcano: Multibeam anomalies and sea—That multibeam sonar comparison, *Geophys. Res. Lett.*, *26*(23), 3425–3428.

Embley, R. W., W. W. Chadwick, M. R. Perfit, M. C. Smith, and J. R. Delaney (2000), Recent eruptions on the CoAxial segment of the Juan de Fuca Ridge: Implications for mid-ocean ridge accretion processes, *J. Geophys. Res.*, *105*(B7), 16,501–16,525.

Fox, C. G., and R. P. Dziak (1998), Hydroacoustic detection of volcanic activity on the Gorda Ridge, February–March 1996, *Deep Sea Res., Part II*, *45*, 2513–2530.

Fox, C. G., W. W. Chadwick, and R. W. Embley (1992), Detection of changes in ridge-crest morphology using repeated multibeam sonar surveys, *J. Geophys. Res.*, *97*(B7), 11,149–11,162.

Fox, C. G., W. W. Chadwick, and R. W. Embley (2001), Direct observation of a submarine volcanic eruption from a sea-floor instrument caught in a lava flow, *Nature*, *412*, 727–729.

Gregg, T. K. P., and J. H. Fink (1995), Quantification of submarine lava-flow morphology through analog experiments, *Geology*, *23*(1), 72–76, doi:10.1130/0091–7613(1995)023<0073.

Griffiths, R. W., and J. Fink (1992), Solidification and morphology of submarine lavas: A dependence on extrusion rate, *J. Geophys. Res.*, *97*(B13), 729–737.

Helfrich, K. R. (1995), Thermo-viscous fingering of flow in a thin gap: A model of magma flow in dikes and fissures, *J. Fluid Mech.*, *305*, 219–238.

Larsen, G. (1984), Recent volcanic history of the VeidIvötn fissure swarm, southern iceland—An approach to volcanic risk assessment, *J. Volcanol. Geotherm. Res.*, *22*, 33–58.

Mattsson, H. B., and Á. Höskuldsson (2011), Contemporaneous phreatomagmatic and effusive activity along the Hverfjall eruptive fissure, north Iceland: Eruption chronology and resulting deposits, *J. Volcanol. Geotherm. Res.*, *201*, 241–252, doi:10.1016/j.jvolgeores.2010.05.015.

Moore, J. G., and H. L. Krivoy (1964), The 1962 flank eruption of Kilauea volcano, *J. Geophys. Res.*, *69*(10), 2033–2045.

Moore, R. B., R. T. Helz, D. Dzurisin, P. W. Gordon, R. Y. Koyanagi, P. W. Lipman, J. P. Lockwood, and G. S. Puniwai (1980), The 1977 eruption of Kilauea volcano, Hawaii, *J. Volcanol. Geotherm. Res.*, *7*, 189–210.

Parcheta, C. E., B. F. Houghton, and D. A. Swanson (2012), Hawaiian fissure fountains 1: Decoding deposits—Episode 1 of the 1969–1974 Mauna Ulu eruption, *Bull. Volcanol.*, *74*, 1729–1743, doi:10.1007/s00445-012-0621-1.

Pollard, D. D., O. H. Muller, and D. R. Dockstader (1975), The form and growth of fingered sheet intrusions, *Geol. Soc. Am. Bull.*, *86*(3), 351–363, doi:10.1130/0016–7606(1975)86<351.

Pollard, D. D., P. Segall, and P. T. Delaney (1982), Formation and interpretation of dilatant echelon cracks, *Geol. Soc. Am.*

Bull., *93*(12), 1291–1303, doi:10.1130/0016–7606 (1982) 93<1291.

Riddihough, R. (1984), Recent movements of the Juan de Fuca plate system, *J. Geophys. Res.*, *89*(B8), 6980–6994, doi:10.1029/JB089iB08p06980.

Rubin, M. (1992), Dike-induced faulting and graben subsidence in volcanic rift zones, *J. Geophys. Res.*, *97*(B2), 1839–1858.

Rubin, A. M. (1993), Tensile fracture of rock at high confining pressure: Implications for dike propagation, *J. Geophys. Res.*, *98*(B9), 15,919–15,935, doi:10.1029/93JB01391.

Rubin, A. M. (1995), Propagation of magma-filled cracks, *Annu. Rev. Earth Planet. Sci.*, *23*, 287–336.

Rubin, K. H., M. C. Smith, M. R. Perfit, D. M. Christie, and L. F. Sacks (1998), Geochronology and geochemistry of lavas from the 1996 North Gorda Ridge eruption, *Deep Sea Res., Part II*, *45*, 2571–2597, doi:10.1016/S0967-0645(98)00084-8.

Rubin, K. H., M. C. Smith, E. C. Bergmanis, M. R. Per, J. M. Sinton, and R. Batiza (2001), Geochemical heterogeneity within mid-ocean ridge lava flows: Insights into eruption, emplacement and global variations in magma generation, *Earth Planet. Sci. Lett.*, *188*, 349–367.

Rubin, K. H., S. A. Soule, D. J. Fornari, D. A. Clague, R. W. Embley, and D. W. Caress (2012), Volcanic eruptions in the deep sea, *Oceanography*, *25*(1), 142–157.

Sinton, J., E. Bergmanis, K. Rubin, R. Batiza, T. K. P. Gregg, K. C. Macdonald, and S. M. White (2002), Volcanic eruptions on mid-ocean ridges: New evidence from the superfast spreading East Pacific Rise, 17°–19°S, *J. Geophys. Res.*, *107*(B6), ECV 3-1–ECV 3–20, doi:10.1029/2000JB000090.

Sinton, J., K. Grönvold, and K. Saemundsson (2005), Postglacial eruptive history of the western volcanic zone, Iceland, *Geochem. Geophys. Geosyst.*, *6*, Q12009, doi:10.1029/2005GC001021.

Smith, D. K., and J. R. Cann (1990), Hundreds of small volcanoes on the median valley floor of the Mid-Atlantic Ridge, *Nature*, *348*, 152–155.

Smith, D. K., and J. R. Cann (1992), The role of seamount volcanism in crustal construction and the Mid-Atlantic ridge, *J. Geophys. Res.*, *97*(B2), 152–155.

Smith, D. K. et al. (1995a), Mid-Atlantic ridge volcanism from deep-towed side-scan sonar images, 25 degrees–29 degrees-N, *J. Volcanol. Geotherm. Res.*, *67*, 233–262.

Smith, D. K., S. E. Humphris, and W. B. Bryan (1995b), A comparison of volcanic edifices at the Reykjanes ridge and the Mid-Atlantic ridge at 24 degrees–30 degrees N, *J. Geophys. Res.*, *100*(B11), 22,485–22,498.

Soule, S. A., D. J. Fornari, M. R. Perfit, and K. H. Rubin (2007), New insights into mid-ocean ridge volcanic processes from the 2005–2006 eruption of the East Pacific Rise, 9°46′N–9°56′N, *Geology*, *35*, 1079–1082, doi:10.1130/G23924A.1.

Soule, S. A., J. Escartín, and D. J. Fornari (2009), A record of eruption and intrusion at a fast spreading ridge axis: Axial summit trough of the East Pacific Rise at 9–10°N, *Geochem. Geophys. Geosyst.*, *10*(10), Q10T07, doi:10.1029/2008GC002354.

Thordarson, T., and S. Self (1993), The Laki (Skaftár Fires) and Grímsvötn eruptions in 1783–1785, *Bull. Volcanol.*, *55*, 233–263.

Touvet, T., N. J. Balmforth, R. V. Draster, and B. R. Sutherland (2011), Fingering instability in buoyancy-driven fluid-filled cracks, *J. Fluid Mech.*, *672*, 60–77, doi:10.1017/S0022112010005860.

White, S. M., K. C. Macdonald, and R. M. Haymon (2000), Basaltic lava domes, lava lakes, and volcanic segmentation, *J. Geophys. Res.*, *105*(B10), 23,519–23,536.

Wylie, J. J., K. R. Helfrich, B. Dade, J. R. Salzig, and J. R. Lister (1999), Flow localization in fissure eruptions, *Bull. Volcanol.*, *60*, 432–440.

Yeo, I., R. C. Searle, K. L. Achenbach, L. Bas, P. Tim, and B. J. Murton (2012), Eruptive hummocks: Building blocks of the upper ocean crust, *Geology*, *40*(1), 91–94.

Zellmer, G., K. Rubin, K. Gronvold, and Z. Juradochichay (2008), On the recent bimodal magmatic processes and their rates in the Torfajökull–Veidivötn area, Iceland, *Earth Planet. Sci. Lett.*, *269*, 388–398, doi:10.1016/j.epsl.2008.02.026.

Ziv, A., and A. M. Rubin (2000), Formation and interpretation of dilatant echelon cracks, *J. Geophys. Res.*, *105*(B3), 5947–5961.